Tellus (1982), *34*, 358–368

An instability study of the onset-vortex of the southwest monsoon, 1979

By MANKIN MAK and C.-Y. JIM KAO, *Laboratory for Atmospheric Research, University of Illinois, 1101 W. Springfield, 6-109 Coordinated Science Laboratory, Urbana, IL 61801, U.S.A.*

(Manuscript received June 1; in final form October 13, 1981)

ABSTRACT

A dry two-layer linear-balanced model is used to investigate the relative effects of the horizontal and vertical shears of the zonal flow over the Arabian Sea in the early phase of the onset of the southwest monsoon in 1979. The basic state is obtained from the MONEX data. Two aspects of the cyclogenesis which immediately preceded the onset of the monsoon can be adequately accounted for by the process of dynamic instability mainly associated with the horizontal shear of the basic flow. These two aspects are the growth rate and the scale selection of the disturbance. To this extent, the results of this study agree with Krishnamurti et al. (1981). But the mainly barotropic instability mechanism incorrectly predicts two other aspects of the cyclogenesis. The maximum intensity of the disturbance is predicted on the southern flank of the jet and the vertical extent of the disturbance is essentially confined to the lower troposphere. These discrepancies reflect the limitations of a dry model.

The vertical shear and stratification significantly influence the structure of the disturbance although their effect on the growth rate is small. The comparison of the linear-balanced model results with the quasi-geostrophic model results suggests that the full variation of the Coriolis parameter with latitude should be retained in future modeling of the onset-vortex.

1. Introduction

The past descriptive accounts of the onset of the southwest monsoon suggest that the usual triggering process is likely to be the formation of a cyclonic vortex over the south-central Arabian Sea (Krishnamurti et al., 1981, to be referred as K81). One such vortex was also observed immediately prior to the onset of the monsoon in 1979 during the Summer Monsoon Experiment, MONEX (Fein and Kuettner, 1980). Such a vortex has been unofficially referred to as an Onset-Vortex in recognition of its unique role in the onset phenomenon. It is therefore of general interest to delineate the nature of its dynamical properties. Since the vortex was observed shortly after the low level westerly flow had intensified (see Fig. 8 in K81), it is reasonable to wonder whether the onset-vortex might at least partly arise from a dynamical instability process of the jet. A barotropic model was used in K81 in conjunction with the most comprehensive available wind data to explore this possibility. These authors specifically examined the stability of the objectively analyzed zonal wind data in the 850–900 mb layer over the Arabian Sea around the period of formation of the onset-vortex (June 9 to June 17, 1979). Their barotropic growth rate computations lend support to the notion that barotropic instability could be a significant process for the initiation of that vortex. Unfortunately, no comparison was made in K81 of the modal structure of their barotropic model unstable disturbance with the actual horizontal flow field. Instead they went on to make a numerical prediction experiment with a strictly barotropic model. The 48-h simulation of the 850 mb flow (from June 13 to June 15) predicts a pronounced vortex somewhat resemblant of the observed vortex (see their Figs. 15, 16 and 17). The major discrepancy is that the simulated vortex is about 4 degrees latitude and longitude to the southeast of the vortex in the verification map.

To fully investigate the dynamical origin of this onset-vortex, one logically should examine not only

0040-2826/82/040358-16$02.50/0

the role of barotropic shear but also the roles of baroclinic shear and moist convection. This type of general analysis was attempted by Shukla (1978) in his study of the monsoon depressions. His model computations support the general notion that moist convection plays an indispensible role in the initiation of a monsoon depression. However, the quantitative effect of moist convection was not unambiguously demonstrated in that analysis, even though the complex parameterization scheme of Arakawa and Shubert (1974) was used. The growth rate of the disturbance in Shukla's model turns out to be monotonically increasing for decreasing wavelength (see his Fig. 4). Only by invoking an additional hypothesis could he interpret the results in terms of monsoon depressions. This puzzling result might reflect the occurrence of conditional instability of the first kind in the model rather than conditional instability of the second kind (Mak, 1981). The nature of interaction between convective clouds and a large scale system is still poorly understood. There has been a growing awareness that an adequate parameterization scheme for large-scale tropical disturbances should probably include the effect of momentum transport by the clouds (e.g., Stevens et al., 1977; Gray, 1979; Mak, 1980). Existing parameterization schemes do not seem to be sufficiently general for making a comprehensive study of the moist convection during the initiation of the onset-vortex. It might be more fruitful for one to first analyze the unique MONEX data for the purpose of identifying the dominant features during the interaction between the vortex and the cloud field.

Saha, Sanders and Shukla (1981) used climatological evidence to demonstrate that a large percentage of the lows and depressions that formed in the Bay of Bengal were associated with predecessor disturbances coming from the east. One might therefore also wonder if the onset-vortex could be associated with a predecessor disturbance in the upstream region, namely off the Somali Coast of East Africa. Since the data for the region is quite sparse even during MONEX, it is not possible to make a definite statement on this possibility. A more indirect evidence however is known and does not lend support to this possibility. The Arabian Sea area-averaged value of the zonal kinetic energy in a domain from 20° N to 4° S, and from 50° E to 70° E was computed in K81 (see their Fig. 7). These authors also computed the zonally averaged meridional velocity throughout the time period (see their Fig. 12). Both results indicate dramatic increase from about June 12, 1979 onward. A reasonable inference is that even assuming the onset-vortex was associated with an upstream disturbance, such a disturbance must have been very weak and must have experienced a rapid intensification over the Arabian Sea. For practical consideration, the incipient onset-vortex disturbance is then more likely an in situ amplifying disturbance.

This investigation has a relatively limited scope. We extend an instability analysis such as that in K81 by considering both the observed horizontal and vertical shears. We will do so with a linear-balanced model for reasons to be elaborated on shortly. The required specification of the basic state stratification may be determined from the temperature data measured by the dropwindsondes during MONEX. The specific objective of the analysis is twofold. We aim at determining the relative roles of the observed vertical and horizontal shears in the absence of moist convection. We also intend to find out if it would be possible to obtain a gross estimate of the three-dimensional structure of the onset-vortex on the basis of the dynamical model disturbance. Such information would complement the ongoing observational and numerical studies of other researchers involved in the MONEX program. Dictated by the availability of the analyzed wind fields, we employ a two-level model for this investigation. The formulation of this model and the extent of validity of the approximations are discussed in Section 2. The results are presented in Section 3.

2. Formulation of the model

The first question to be addressed is whether a fully non-geostrophic model is needed for analyzing the onset-vortex. The answer depends largely upon the range of expected values for the Richardson number Ri of the basic state. Stone (1966, 1970) analyzed baroclinically unstable disturbances in a f-plane model over a wide range of Ri values. He showed that the unstable disturbances for Ri as as small as $O(10)$ are qualitatively similar to the quasi-geostrophic disturbances for $Ri \approx O(10^2)$. Only when Ri is of $O(1)$ would basically different disturbances become most unstable. We can readily make a crude estimate of Ri for the Arabian Sea region during the period of formation of the onset-vortex. The maximum zonal wind at 850 mb before June 15, 1979 was about 15 m s^{-1} and that at 200 mb was about -5 m s^{-1}. The overall tropospheric vertical shear is therefore about 3 m s^{-1} (100 mb)$^{-1}$. The static stability

$$S \equiv \frac{-R}{P}\left(\frac{\partial T}{\partial p} - \frac{RT}{c_p p}\right)$$

may be estimated from the temperature data measured by the MONEX dropwindsondes. We found that a typical value of S in mid-troposphere is about 0.027 m^2 s^{-2} mb^{-2}. It follows that the Richardson number is about $Ri = S/(\partial u/\partial p)^2 \approx 30$. Hence, if 3 m s^{-1} (100 mb)$^{-1}$ is a realistic estimate of the vertical shear, the non-geostrophic effects would not be expected to be large. Another way of viewing this is that the non-geostrophic effects would be important only if the local maximum vertical shear turns out to be about five and a half times as large as the value estimated above (i.e., $\partial u/\partial p \approx 16$ m s^{-1} (100 mb)$^{-1}$ would lead to $Ri \approx 1$). Such a large shear is not probable.

Although the non-geostrophic effects due to the vertical advection of momentum and horizontal advection of heat and momentum by the divergent part of the flow are not expected to be strong, it may not be adequate to use a familiar quasi-geostrophic model (e.g., Pedlosky, 1979, Section 7.2) for investigating the onset-vortex which was located at fairly low latitudes. Observations indicated that the disturbance was first found centering at about 9° N (Sikka and Grossman, 1980). Considering the horizontal extent of the disturbance, we anticipate that part of it would be over the equatorial latitudes. Thus, a cross-equatorial domain should be used in making a model analysis. The percentage variation of the Coriolis parameter with latitudes is large in such a domain. To specifically take this aspect into consideration, we adopt the model first proposed by Lorenz (1960). The variation of the Coriolis parameter with latitude is retained whenever it appears in the governing equations. Recent applications of this model to studying the effects of spherical geometry on baroclinic instability indicate that the solutions do not manifest gross distortion over the equator (Hollingsworth, 1975; Frederiksen, 1978). This model framework therefore seems to be appropriate for analyzing the onset-vortex-like disturbances. This model is a version of the so-called linear-balanced model and will thus be referred to as the LB model in the subsequent discussion. Counterpart computations have also been made with a familiar quasi-geostrophic model (QG model) for the purpose of comparison (Kao, 1981).

Introducing the notation ψ the stream-function, χ the velocity potential, ϕ the geopotential, T the temperature and ω the p-velocity, we can write the governing equations for inviscid adiabatic motions in the LB model as

$$\frac{\partial}{\partial t}\nabla^2\psi = -J(\psi, \nabla^2\psi + f) - \nabla\cdot(f\nabla\chi) \tag{1}$$

$$\frac{\partial T}{\partial t} = -J(\psi, T) + \hat{S}\omega \tag{2}$$

$$\frac{\partial \phi}{\partial p} = -\frac{RT}{p} \tag{3}$$

$$\nabla^2\chi + \frac{\partial\omega}{\partial p} = 0 \tag{4}$$

$$\nabla^2\phi - \nabla\cdot(f\nabla\psi) = 0 \tag{5}$$

where J denotes the Jacobian, ∇ the gradient operator, p the pressure as a vertical coordinate, R the gas constant,

$$\hat{S} = -\left(\frac{d\hat{T}}{dp} - \frac{R\hat{T}}{c_p p}\right)$$

with $\hat{T}$ the horizontal mean temperature regarded as being fixed. As pointed out by Lorenz, these equations conserve the sum of kinetic energy and available potential energy, but do not describe the relation between static stability and energy. For the horizontal dimension of the onset-vortex, it suffices to use a local Cartesian coordinate for the region between 20° N and 10° S. Hence, we use

$$\nabla = \frac{\partial}{\partial x}\mathbf{i} + \frac{\partial}{\partial y}\mathbf{j} \tag{6}$$

$$f = f_0 + \beta y \tag{7}$$

$\mathbf{i}$ and $\mathbf{j}$ are unit vectors pointing eastward and northward. f_0 is the value of the Coriolis parameter evaluated at the center of the domain, $y = 0$ set at 5° N. β is df/dy evaluated at $y = 0$. The meridional domain is $-Y \leqslant y \leqslant Y$ with $Y = r_0\,\pi/12$ where r_0 is the radius of the earth. The choice for the center-latitude is not unique, and turns out not to be critical. It was the center of the latitudinal domain where we could determine the basic flow with most confidence. It was also somewhat compatible with the observation that the onset-vortex was first observed at 9° N (Sikka and Grossman, 1980). The sensitivity of the results to the choice of the center-latitude can be readily checked. It will be commented on in Section 3.

The basic state is characterized by a general zonal flow $\bar{u}\ (y,p)$ and a stable stratification $\bar{S} > 0$. The particular structure of this basic state is to be deduced from the available MONEX data. It follows that the basic χ, ψ and ϕ fields are related to $\bar{u}$ by

$$\bar{\chi} = 0 \tag{8}$$

$$\frac{\partial \bar{\psi}}{\partial y} = -\bar{u} \tag{9}$$

$$\frac{\partial \bar{\phi}}{\partial y} = -f\bar{u} \tag{10}$$

In conjunction with this basic state, we consider small amplitude perturbations which are denoted by ψ', χ', ϕ', T', and ω'. These quantities are governed by the linearized versions of (1) to (5). Upon eliminating T', we obtain (after dropping the prime notation)

$$\nabla^2 \psi_t = -\bar{u}\nabla^2 \psi_x + \bar{u}_{yy}\,\psi_x - f\nabla^2 \chi - (\psi_x + \chi_y)\,\beta \tag{11}$$

$$\phi_{pt} = -\bar{u}\phi_{px} + f\bar{u}_p\,\psi_x - S\omega \tag{12}$$

$$\nabla^2 \chi + \frac{\partial \omega}{\partial p} = 0 \tag{13}$$

$$\nabla^2 \phi - f\nabla^2 \psi - \beta\psi_y = 0 \tag{14}$$

where $S = (R/p)\,\bar{S}$. Relationships (3), (9) and (10) have been used in deriving (12). The subscripts above denote partial derivatives. Cyclical boundary condition in the x direction is used for simplicity. We may then seek a normal mode solution of the form

$$a(x,y,p,t) = A(y,p)\,e^{ik(x-ct)} \tag{15}$$

where a can be ψ, ϕ, χ or ω. The amplitude functions for these quantities are respectively denoted as Ψ, Φ, Λ, and W. They are then to satisfy the following equations obtained from (11) to (14):

$$\{ik(\bar{u}-c)\frac{\partial^2}{\partial y^2} + ik[-k^2(\bar{u}-c) + \beta - \bar{u}_{yy}]\}\,\Psi + \beta\frac{\partial \Lambda}{\partial y} - f\frac{\partial W}{\partial p} = 0 \tag{16}$$

$$-ikf\bar{u}_p\,\Psi + ik(\bar{u}-c)\frac{\partial \Phi}{\partial p} + SW = 0 \tag{17}$$

$$\left(\frac{\partial^2}{\partial y^2} - k^2\right)\Lambda + \frac{\partial W}{\partial p} = 0 \tag{18}$$

$$\left\{-f\frac{\partial^2}{\partial y^2} - \beta\frac{\partial}{\partial y} + fk^2\right\}\Psi + \left(\frac{\partial^2}{\partial y^2} - k^2\right)\Phi = 0 \tag{19}$$

Analyzed streamlines and isotahs for the Arabian Sea region are presently available only at three levels—200, 700 and 850 mb (Krishnamurti et al., 1979). We can therefore only use a two-layer model. To assess how detrimental the use of this crude vertical resolution might be, we may consider an analogous analysis by Shukla (1977). He used a 10-level quasi-geostrophic model to investigate the stability of the July mean monsoon flow over the Bay of Bengal. This flow has strongest vertical shear at about 10° N and largest horizontal shear at about 25° N above the mid-troposphere. Shukla's computations showed that the model unstable disturbance mainly arises from barotropic instability processes in the upper troposphere. The amplitude of the unstable disturbance is confined to a relatively thin layer although the model has sufficient vertical resolution to depict a broader structure. One might infer that had he used fewer levels in the model, he would have essentially reached the same conclusion provided that the horizontal shear is adequately represented.

The levels in the model are indicated by an index j ($j = 0, 1, 2, 3, 4$) corresponding to pressure $p_j = p_4 - (4 - j)\Delta p$ with $\Delta p = (p_4 - p_0)/4$. For energetic consistency consideration, Ψ, Λ and Φ are defined at levels 1 and 3 and eq. (17) at level 2. This leads to seven ordinary differential equations that govern the seven unknowns: W_2 and Ψ_l, Λ_l, Φ_l ($l = 1, 3$). The vertical boundary conditions may be taken as $W_0 = W_4 = 0$ which imply

$$\Lambda_3(y) = -\Lambda_1(y) \tag{20}$$

Thus, we effectively have six equations to be solved. We can further eliminate W_2 among these six independent equations, reducing them finally to a system of five equations as follows.

$$\left[(\bar{u}_1 - c)\frac{d^2}{dy^2} - k^2(\bar{u}_1 - c) + \beta - \bar{u}_1''\right]\Psi_1 + \left[(\bar{u}_3 - c)\frac{d^2}{dy^2} - k^2(\bar{u}_3 - c) + \beta - \bar{u}_3''\right]\Psi_3 = 0 \tag{21}$$

$$-\frac{ikf}{2(\Delta p)^2}(\bar{u}_3 - \bar{u}_1)(\Psi_1 + \Psi_3) + \frac{ik}{(\Delta p)^2} \times \left(\frac{\bar{u}_1 + \bar{u}_3}{2} - c\right)(\Phi_3 - \Phi_1) + S\left(k^2 - \frac{d^2}{dy^2}\right)\Lambda_1 = 0 \tag{22}$$

$$ik\left[(\bar{u}_3 - c)\frac{d^2}{dy^2} - k^2(\bar{u}_3 - c) + \beta - \bar{u}_3''\right]\Psi_3 + \left[-f\frac{d^2}{dy^2} - \beta\frac{d}{dy} + fk^2\right]\Lambda_1 = 0 \tag{23}$$

$$\left[-f\frac{d^2}{dy^2} - \beta\frac{d}{dy} + fk^2\right]\Psi_1 + \left(\frac{d^2}{dy^2} - k^2\right)\Phi_1 = 0 \tag{24}$$

$$\left[-f\frac{d^2}{dy^2} - \beta\frac{d}{dy} + fk^2\right]\Psi_3 + \left(\frac{d^2}{dy^2} - k^2\right)\Phi_3 = 0 \tag{25}$$

where $\bar{u}_l'' = d^2\bar{u}_l/dy^2$ $(l = 1, 3)$. The lateral boundary conditions at $y = \pm Y$ are prescribed as follows. For an instability study, we may consider the meridional domain to be within two rigid boundaries. We therefore require the meridional velocity to be zero at $y = \pm Y$. Specifically, the divergent and rotational parts of v are required to be individually zero at $y = \pm Y$. This implies

$$\Psi_1(\pm Y) = \Psi_3(\pm Y) = \text{constant} = 0 \tag{26}$$

$$\left.\frac{d\Lambda}{dy}\right|_{\pm Y} = 0 \tag{27}$$

The boundary conditions for ϕ may be obtained from the geostrophic relation

$$-\frac{\partial\phi}{\partial x} + fv = 0 \tag{28}$$

Since $v = 0$ at $y = \pm Y$, we then have

$$\Phi_1(\pm Y) = \Phi_3(\pm Y) = \text{constant} = 0 \tag{29}$$

The five equations (21) to (25) for five unknowns with ten boundary conditions (26), (27), and (29) constitute a two-point boundary value problem. c is the eigenvalue; Ψ_1, Ψ_3, Φ_1, Φ_3 and Λ_1 together form the eigenfunction. This problem is to be solved numerically using a grid resolution of one-degree latitude. We introduce the approximation of expressing the derivatives in eqs. (21) to (25) in a centered difference form and the derivative in the boundary condition (27) in an uncentered difference form. The resulting algebraic equations can be put into a simple matrix form. They can then be readily solved with the use of a direct inversion method. With this grid resolution, we will have to deal with matrices of size 150 by 150. The computer memory requirement for using this LB model is considerably larger than that for the QG model. If we had used more vertical levels in the model, the corresponding matrices would have been prohibitively large for using the direct method. An initial value problem approach may then be more feasible.

3. Results

According to the Summer MONEX Atlas (Krishnamurti et al., 1979, pp. 108–140) the 200 mb streamlines and isotahs in the region of interest indicate a basically broad easterly flow throughout the period from June 10 to June 18, 1979. A large anticyclonic system was noted over the Arabian Peninsula, but it was never over the Arabian Sea region and was not associated with the onset-vortex at low levels. Another relevant observational source is the wind atlas constructed on the basis of the geostationary satellite images (Young et al., 1980). The "upper layer" wind (300–100 mb layer wind) in this atlas also did not show systematic anticyclonic curvature over the Arabian Sea area in the period of June 10–18, 1979 (see pp. 41–49). Hence, both the conventional data and the satellite data suggest that the disturbance's amplitude must be very weak at the 200 mb level. On this basis, we chose p_0 = 200 mb as the top level of the model. The basic flow $\bar{u}_1$ and $\bar{u}_3$ at 400 mb and 800 mb are determined as follows. The values of the wind direction and speed on a set of 5° by 5°

grids overlaid upon the region between 10° S and 20° N, and between 50° E and 80° E are read off from the Summer MONEX Atlas. We do so for the 850 and 200 mb levels in the period from June 10 to June 16, 1979, during which the onset-vortex is known to form. The zonal averaging of these wind data for each day gives a daily meridional profile of the mean zonal flow. The profile obtained on the 850 mb level is directly used as the basic flow level, $\bar{u}_3$. The data are not so precise so as to warrant a slight modification in order to correct for the difference between the actual flow at 850 and 800 mb. The profile for $\bar{u}_1$ is obtained by means of a linear interpolation in pressure on the basis of the $\bar{u}$ profiles for the 200 and 850 mb levels. Fig. 1 shows the profiles $\bar{u}_1$ and $\bar{u}_3$ on June 10, 11, 12 and 13 of 1979, and the 4-day average profiles (curves labelled A and B). The latter may be regarded as the overall basic flow shortly before the onset of monsoon began at the southern tip of India on June 13, 1979. Fig. 1 shows a gradual strengthening of the low level westerly jet. The upper level zonal flow in this period was easterly and had relatively small meridional shears. Fig. 2 shows the basic flows on June 14, 15 and 16. The low-level jet effectively stopped increasing on those days. The onset-vortex was noticeable on the weather maps by then. The maximum speed of the jet is seen to be about 18 m s^{-1}. As mentioned before, the dropwindsonde temperature data is used to compute the static stability parameter S. A mean value of S is found to be 0.027 m^2 mb^{-2} s^{-2} for the mid-tropospheric levels.

We first make the eigenvalue–eigenfunction computations for the 4-day average of the profiles of June 10, 11, 12 and 13, as shown by the curves with labels A and B in Fig. 1. Fig. 3 shows the results of the growth rate and the phase speed as a function of the wavelength of the disturbance. It is seen that the flow is weakly unstable with a maximum growth rate of about 1.5×10^{-6} s^{-1} (e-folding time of ~8 days), and a phase speed of -2 m s^{-1} for a wavelength of about 3500 km. We next examine the instability properties of the individual daily basic flows. These computations are meaningful to the extent that they would give us some indication as to how the growth rate of the vortex might vary during the initial period of development. Strictly speaking, this methodology is not suitable for analyzing a time varying basic state. This procedure would of course be completely unjustifiable if the variation of the basic flow is itself a consequence of the feedback effect of the unstable wave. This is however not the case here because the progressive strengthening of the jet appears to be caused by an upstream meridional pressure gradient (Kuettner and Unninayar, 1980). Furthermore, the variations of the basic flow on June 14, 15 and 16 (Fig. 2) are quite small. Figs. 4a

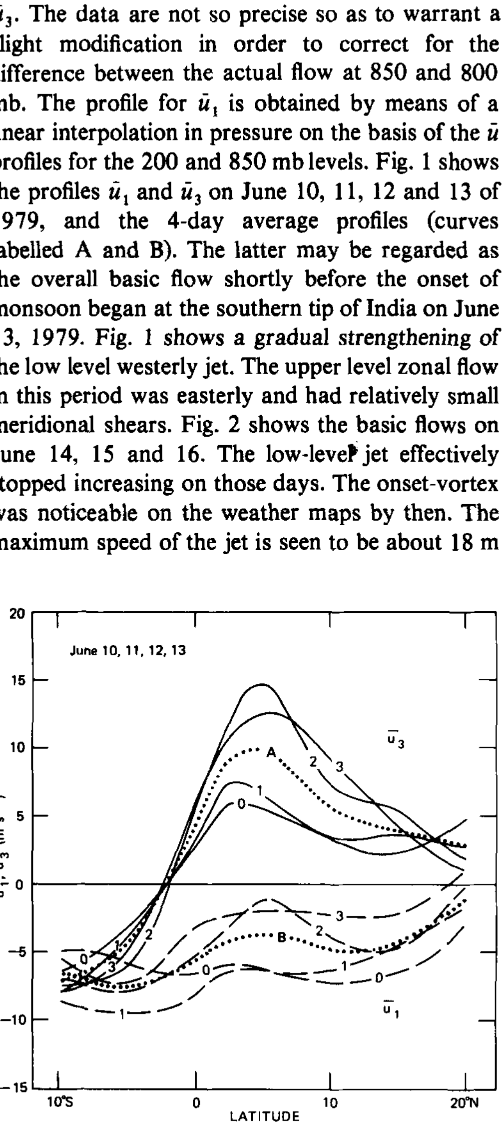

Fig. 1. The meridional profiles of the basic zonal flows, $\bar{u}_1$ (dashed) and $\bar{u}_3$ (solid) on June 10, 11, 12, 13 (labelled 0, 1, 2, 3) in m s^{-1}. The dot curves with labels A or B are the corresponding 4-day average profiles.

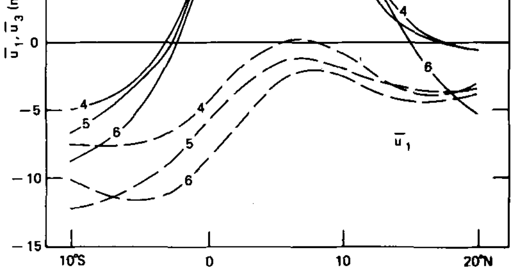

Fig. 2. Same as Fig. 1 for June 14, 15 and 16.

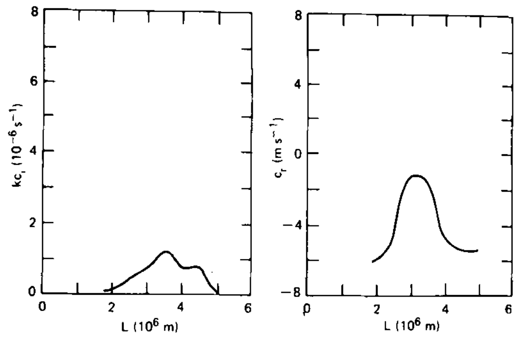

Fig. 3. The variations of the growth rate and phase speed of the disturbance with wavelength for the 4-day average basic flow.

and b show the growth rate results as a function of the wavelength on each day. Figs. 4c and d show the corresponding phase speed results. The curves labelled 0 to 6 refer to June 10 to 16. It is seen from Fig. 4a that the basic flow on June 10 and 11 is rather weakly unstable (1×10^{-6} s^{-1} growth rate) for relatively shorter wavelengths (about 2000 km). The growth rates for June 12 and 13 are progressively larger. Disturbances of longer wavelengths are becoming more unstable. The results in Figs. 4a and c are complementary to those in Fig. 1. As anticipated by the small variations among the profiles for June 14, 15 and 16 (Fig. 2), we find correspondingly small variations in the results of growth rate and phase speed shown in Figs. 4b and d. The results for one of these individual days may be interpreted as the results for the average basic state over the period of developing onset. The maximum growth rate is about 4×10^{-6} s^{-1} for a wavelength of about 3000 km. We have also made computations with a barotropic model using a basic flow identical with the $\bar{u}_3$ profiles used in this model. The eigenvalues in the two models are found to differ by no more than 10%. The corresponding eigenvalues obtained with the QG model are also similar to the results presented above within a few percent. The small differences in the growth rates obtained from the three models attest to the fact that the horizontal shear of the low-level basic flow is the primary factor in giving rise to the instability. The lack of significance of the vertical shear for the growth rate of large-scale disturbances in the tropics has also been found by Kuo (1978) with a variety of shear flows in a primitive-equation model. The basic reason for this is that the required minimum vertical shear for instability in low latitudes is large since this quantity varies with the Coriolis parameter f as $1/f^2$ (Phillips, 1954). However, the stratification and vertical shear may have significant influence on the structure of the perturbation even though they do not significantly affect the growth rate (Kuo, 1978).

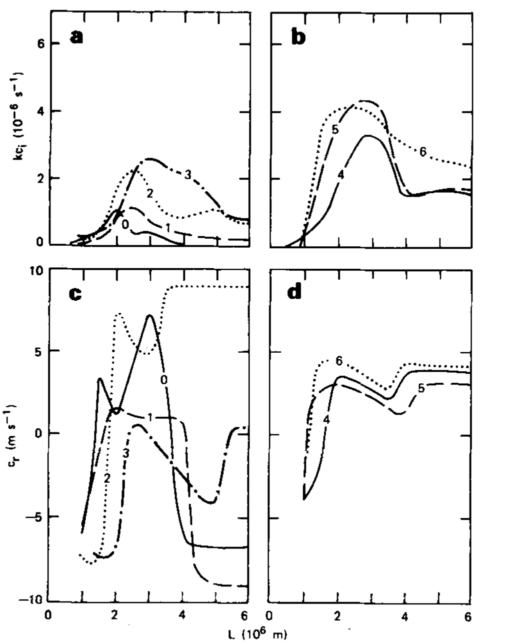

Fig. 4. The variations of the growth rate and phase speed with wavelength for the basic flow of each individual day: (a) growth rate values for June 10, 11, 12, 13; (b) growth rate values for June 14, 15, 16; (c) phase speed values for June 10, 11, 12, 13; and (d) phase speed values for June 14, 15 and 16.

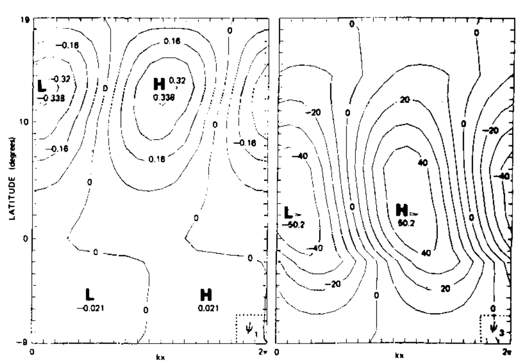

Fig. 5. The structure of the streamfunctions ψ_1 and ψ_3 for the most unstable disturbance for the June 14 basic flow (10^5 m^2 s^{-1}).

The representative properties of the structure of the most unstable mode in this model can be illustrated with that of wavelength 3000 km for June 14. Fig. 5 shows the upper and lower level streamfunctions, ψ_1 and ψ_3. The eigenfunction is arbitrarily normalized to give a maximum speed of 5 m s^{-1} due to the rotational wind. The disturbance shown in Fig. 5 is mainly confined in the lower half of the troposphere. ψ_3 in Fig. 5 has a broad region of maximum amplitude between 2° N and 5° N which is to the south of the jet center of the basic flow rather than on the northern flank of it. This result is an indication of discrepancy between observation and the theoretical explanation which attributes the formation of the onset-vortex to the barotropic instability mechanism. This result is a manifestation of a general property of a barotropically unstable flow first pointed out by Kuo (1978). His computations led to the important conclusion that the maximum intensity of the disturbance would occur on that side of the jet where the absolute vorticity is small. In this case, the southern flank of the jet has smaller absolute vorticity. Therefore, our result is precisely what one would anticipate on the basis of Kuo's general finding. This is also why the numerically simulated vortex with a barotropic model in K81 is noticeably to the south of the observed vortex. Our result then highly suggests that in order to accurately account for the onset-vortex position, additional physical processes, presumably the moist convection, need to be incorporated into the model.

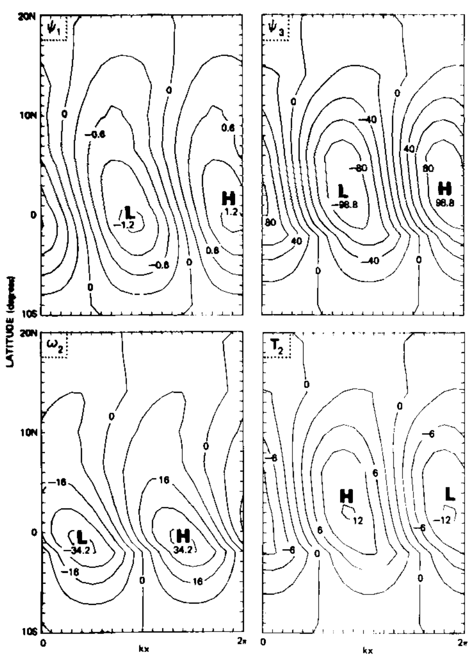

Fig. 6. The structure of the most unstable mode in the QG model for June 14 basic flow. ψ_1 and ψ_3 the upper and lower levels of the streamfunction, unit 10^4 m^2 s^{-1}; ω_2 in units of 10^{-6} mb s^{-1}; T_2 temperature in 10^{-2} °K (taken from Kao, 1981).

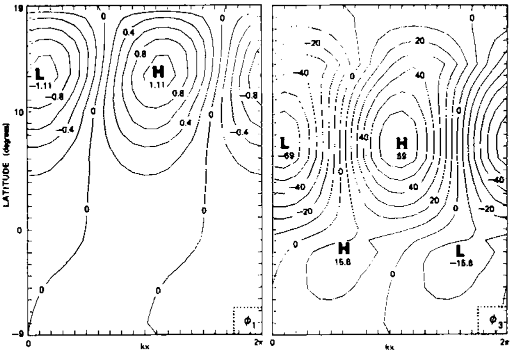

Fig. 7. Same as Fig. 5 except for the geopotential fields ϕ_1 and ϕ_3 (m^2 s^{-2}).

It is worth noting a difference between the vertical structure of the ψ field in the QG model and that in the LB model. The ψ field center in the LB model is located to the north of the ψ_3 center, indicating a northward tilt with height. An opposite tilt is however found in the QG model result as seen in Fig. 6. Fig. 7 shows the geopotential fields ϕ_1 and ϕ_3. The magnitude of ϕ_3 is likewise much larger than that of ϕ_1. ϕ_3 centers on 8° N and ϕ_1 centers on 13° N. It should be noted that the center of ϕ_3 is considerably further north of that of ψ_3. In the subtropical latitudes the ϕ_3 and ψ_3 contours are nearly parallel to one another. This is not so in the equatorial latitudes. The significant relative phase between the ϕ_3 field and the ψ_3 field as seen in Figs. 5 and 7 illustrates another pronounced difference between the LB model and the QG model. In the latter, ϕ is proportional to ψ. Since $\psi_3 \gg \psi_1$, we would have $\phi_3 \gg \phi_1$. It follows that the contours of temperature field, which is proportional to $(\phi_1 - \phi_3)$, are essentially parallel to the contours of ψ_3 in the QG model. The temperature field in this model, shown in Fig. 8, is located significantly north of the ψ_3 field. The warm core of the disturbance is found to be located about four degrees of latitude to the north of the streamfunction center. Corresponding to the normalized

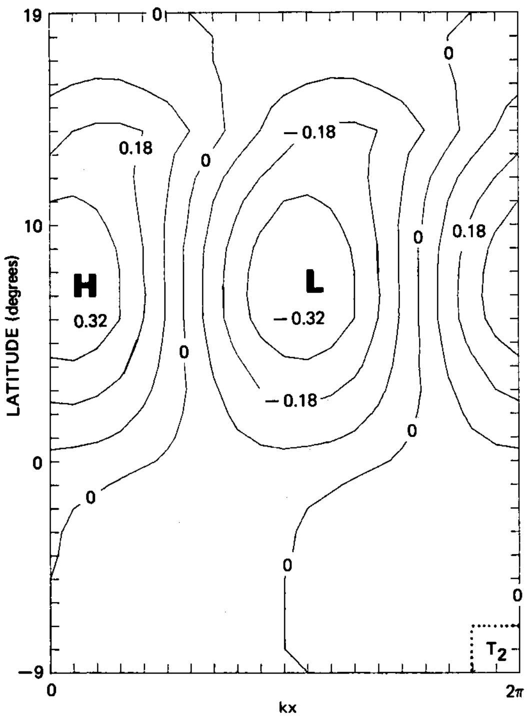

Fig. 8. Same as Fig. 5 except for the temperature field (°C).

minimum wind of 5 m s^{-1}, the maximum temperature is 0.32 °C.

Fig. 9 shows the velocity potential field on the upper level χ_1 and the ω_2 field. It is seen that the ascending motions are located at about 10° N and a quarter wavelength to the west of the low level disturbance center. In contrast, we find that the upward motion region in the QG model is to the southwest of the disturbance center (see Fig. 6). No verification can presently be made with observation since no detailed synoptic analysis of the ω field of the onset-vortex has been reported. The magnitude of ω_2 in the model is very weak, stemming from the absence of baroclinic instability. This is to be expected in a dry model for low latitudes. The smallness of ω_2 is an *a posteriori* indication that the non-geostrophic effects would indeed be small had they been included in the model.

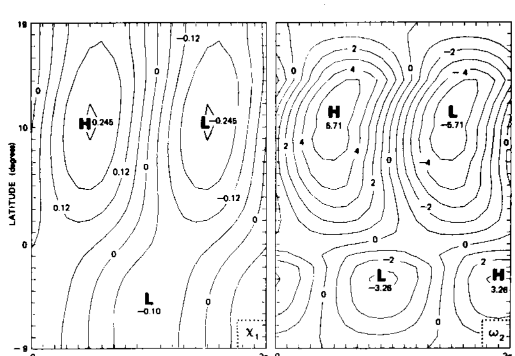

Fig. 9. Same as Fig. 5 except for the velocity potential on level 1 (10^5 m^2 s^{-1}) and the p-velocity field on level 2 (10^{-5} mb s^{-1}).

The energetics of the unstable disturbance in this model are next examined. Let us denote the integration of a quantity r over the mass in the three-dimensional domain within a wavelength in the x direction by $\langle r \rangle$, namely

$$\langle r \rangle = \int_{p_{top}}^{p_{bottom}} \int_{-Y}^{Y} \int_{0}^{L} r \, dx \, dy \, dp/g \tag{30}$$

When we multiply (11) by ψ and integrate the resulting equation over such a domain, we obtain

$$\frac{d}{dt} \langle \tfrac{1}{2} \nabla \psi \cdot \nabla \psi \rangle = \langle \bar{u}_y \, \psi_x \, \psi_y \rangle + \langle f \omega \psi_p \rangle + \langle \psi \chi_y \beta \rangle \tag{31}$$

In obtaining (31), integration by parts has been used in conjunction with the boundary conditions. Likewise, when we multiply (12) by $(1/S)(\partial\phi/\partial p)$ and integrate the resulting equation over that domain, we obtain

$$\frac{d}{dt} \left\langle \frac{(\phi_p)^2}{2S} \right\rangle = \left\langle \frac{f \bar{u}_p}{S} \phi_p (\psi_x + \chi_y) \right\rangle - \langle \omega \phi_p \rangle \tag{32}$$

Equations (31) and (32) are the kinetic energy and the available potential energy budget equations respectively. $\langle \omega \phi_p \rangle$ and $\langle f \omega \psi_p + \psi \chi_y \beta \rangle$ are expected to be equal, representing the conversion from the wave available potential energy to the wave kinetic energy. This can indeed be shown to be so by making use of (13) and (14). We can write

$$\begin{aligned} &\langle f \omega \psi_p + \beta \psi \chi_y \rangle \\ &\quad = \langle (f \omega \psi)_p + \nabla \cdot (f \psi \nabla \chi) - \nabla \cdot (\phi \nabla \chi) - (\phi \omega)_p + \omega \phi_t \\ &\quad = \langle \omega \phi_p \rangle \end{aligned} \tag{33}$$

The last step follows from the fact that each of the other four terms is a divergence of a flux, and individually vanishes by virtue of the boundary conditions. Based on (31), (32) and (33), we can then write the energy budget equations for our model as

$$\frac{1}{2}\frac{d}{dt}([\nabla\psi_1\cdot\nabla\psi_1]+[\nabla\psi_3\cdot\nabla\psi_3])$$
$$=[\bar{u}_{1y}\,\psi_{1x}\,\psi_{1y}]+[\bar{u}_{3y}\,\psi_{3x}\,\psi_{3y}]+\left[\frac{1}{2\Delta p}\,\omega_2(\phi_3-\phi_1)\right] \tag{34}$$

$$\frac{1}{2}\frac{d}{dt}\left[\frac{1}{S}\left(\frac{\phi_1-\phi_3}{2\Delta p}\right)^2\right]$$
$$=\left[\frac{f(\bar{u}_1-\bar{u}_3)}{2S(2\Delta p)^2}(\phi_3-\phi_1)(\psi_{1x}+\psi_{3x})\right]-\left[\frac{1}{2\Delta p}\,\omega_2(\phi_3-\phi_1)\right] \tag{35}$$

where the square bracket denotes integration over one wavelength in the x-direction and the whole meridional extent. Each term on the right-hand sides of (34) and (35) is computed with the eigenfunction of the most unstable mode on June 14. It is found that the term $[\bar{u}_{3y}\,\psi_{3x}\,\psi_{3y}]$ is two orders of magnitude larger than the other terms. This is the energetic manifestation of the barotropic nature of the instability on the low level. From the horizontal tilt of the streamfunction field, one can infer that this kinetic energy transfer from the basic flow to the disturbance takes place strongly on both flanks of the jet. There is also a net conversion from the wave kinetic energy to the wave available potential energy. This reflects the stabilizing effect of the static stability in conjunction with the vertical shear of the basic flow. Such a consequence can be seen from the net out-of-phase relationship between the $-\omega_2$ and the temperature fields in Figs. 8 and 9.

To check the sensitivity of the results to the choice of the center-latitude of the domain, we have repeated the computation using 10° N as the center. Essentially similar results are obtained. We have also repeated the computation using an upper level basic flow based on the 700 and 200 mb data: essentially the same results are also obtained.

4. Concluding remarks

This analysis agrees with the finding of Krishnamurti et al. (1981) to the extent that the growth rate and the preferred length scale of the onset-vortex are largely dependent upon the instability process due to the horizontal shear of the basic flow. Our results however reveal some definite discrepancy with observation. The mainly barotropic instability mechanism predicts the maximum intensity of the disturbance to be on the southern flank of the jet, rather than on the northern flank as observation seems to indicate. This theoretical result is a particular manifestation of a general finding of Kuo (1978) in a primitive-equation model. He found that in situations where barotropic instability prevails the disturbance is located mainly on the side of the jet where the absolute vorticity is small. A discrepancy of similar nature is actually also present in the result of a numerical simulation in Krishnamurti et al. (1981).

The results also indicate that although the vertical shear and stratification do not strongly affect the growth rate, they significantly influence the structure of the model disturbance. In particular, the disturbance is confined to the lower troposphere. The disturbance is located at such low latitudes that the required vertical shear for triggering baroclinic instability far exceeds the estimated vertical shear. Thus, uncertainty in the actual vertical shear should not be a critical factor. While it would be desirable to do an analysis with better vertical resolution than that which we have done, the lack of fine resolution does not qualitatively dictate the results. The non-geostrophic effects are small as evidenced *a posteriori* by the smallness of the vertical velocity field. The linear-balanced model yields a noticeably different meridional tilt with height in the structure of the disturbance than that in a quasi-geostrophic model. The full variation of the Coriolis parameter with latitude should be retained in future modeling.

One can hardly over-exaggerate the need of modeling the moist convection in this problem. Without it, the model cannot correctly predict the meridional position and vertical extent of the onset-vortex, although the growth rate and scale selection aspects can be accounted for by the barotropic instability process. It may well be that the barotropic instability process and the moist convection exert complementary effects in much the same way as they do in producing an Intertropical Convergence Zone as some models have indicated (e.g., Bates, 1970).

In a broader perspective, the onset-vortex formation should be considered in conjunction with the timing of the intensification of the low level westerly jet over the south-central Arabian Sea. The latter is in turn suspected of being dependent upon a number of possible planetary scale factors which have yet to be investigated quantitatively. This study only addresses one facet of the complex onset phenomenon.

5. Acknowledgements

We express our appreciation to Dr. K. Trenberth for reading the manuscript and for his useful comments and suggestions. This research was supported by the GARP, Division of Atmospheric Sciences, National Science Foundation, under grant no. ATM-8019423.

REFERENCES

Arakawa, A. and Schubert, W. H. 1974. Interaction of a cumulus cloud ensemble with the large-scale environment. Part. I. *J. Atmos. Sci. 31*, 674–701.

Bates, J. R. 1970. Dynamics of disturbances on the intertropical convergence zone. *Q. J. Roy. Meteorol. Soc. 96*, 677–701.

Fein, J. and Kuettner, J. 1980. :MONEX', report on the summer field phase. *Bull. Amer. Meteorol. Soc. 61*, 461–475.

Frederiksen, J. S. 1978. Growth rates and phase speeds of baroclinic waves in multi-level models on a sphere. *J. Atmos. Sci. 35*, 1816–1826.

Gray, W. M. 1979. Hurricanes/their formation, structure and likely role in the tropical circulation. *Meteorology over the tropical oceans* (ed. Shaw), *R. Meteorol. Soc.* 155–218.

Hollingsworth, A. 1975. Baroclinic instability of a simple flow on the sphere. *Q. J. Roy. Meteorol. Soc. 101*, 495–528.

Kao, C.-Y. J. 1981. "A barotropic-baroclinic instability study of the onset-vortex of the southwest monsoon in 1979." M.S. thesis, Lab. for Atm. Res., University of Illinois at Urbana-Champaign, Urbana, Illinois, U.S.A.

Krishnamurti, T. N., Ardanuy, P., Ramanathan, Y. and Pasch, R. 1979. Quick look "summer MONEX atlas". Part II. The onset phase. Florida State University Report No. 79-5, Tallahasee, Florida, U.S.A.

Krishnamurti, T. N., Ardanuy, P., Ramanathan, Y. and Pasch, R. 1981. On the onset vortex of the summer monsoon. *Mon. Wea. Rev. 109*, 344–363.

Kuettner, J. P. and Unninayar, M. S. 1980. The near equatorial jet south of India and its role in the onset of the monsoon. *GARP FGGE operations report, vol 9*, W. M. O., Geneva, Switzerland.

Kuo, H. L. 1978. A two-layer model study of the combined barotropic and baroclinic instability in the tropics. *J. Atmos. Sci. 35*, 1840–1860.

Lorenz, E. N. 1960. Energy and numerical weather prediction. *Tellus 12*, 364–373.

Mak, M.-K. 1980. On the growth of the hurricane depression induced by cumulus momentum mixing. 13th Technical Conference on Hurricanes and Tropical Meteorology, Miami, Florida, U.S.A. Abstract in *Bull. Amer. Meteorol. Soc. 61*, 1124.

Mak, M.-K. 1981. An inquiry on the nature of CISK. *Tellus 33*, 531–537.

Pedlosky, J. 1979. *Geophysical fluid dynamics*. Springer-Verlag, 624 pp.

Phillips, N. A. 1954. Energy transformation and meridional circulations associated with simple baroclinic waves in a two-level, quasi-geostrophic model. *Tellus 6*, 273–286.

Saha, K., Sanders, F. and Shukla, J. 1981. Westward propagating predecessors of monsoon depressions. *Mon. Wea. Rev. 109*, 330–343.

Shukla, J. 1977. Barotropic-baroclinic instability of mean zonal wind during summer monsoon. *Pure and Applied Geophysics* (PAGEOPH) *115*, 1449–1461.

Shukla, J. 1978. CISK-barotropic-baroclinic instability and the growth of monsoon depressions. *J. Atmos. Sci. 85*, 495–508.

Sikka, D. R. and Grossman, B. 1981. A chronological weather summary for summer MONEX. *GARP FGGE Operations Report Vol. 8, Appendix 2.1.*

Stevens, D. E., Lindzen, R. S. and Shapiro, L. J. 1977. A new model of tropical waves incorporating momentum mixing by cumulus convection. *Dyn. of Atmos. and Oceans 1*, 365–425.

Stone, P. H. 1966. On nongeostrophic baroclinic instability, Part I. *J. Atmos. Sci. 23*, 1515–1525.

Stone, P. H. 1970. On nongeostrophic baroclinic instability, Part II. *J. Atmos. Sci. 27*, 721–726.

Young, J. A., Virji, H., Wyle, D. P. and Lo, C. 1980. *Summer monsoon windsets from geostationary satellite data.* Dept. of Meteorology, University of Wisconsin, Madison, Wisconsin, U.S.A., 127 pp.